JPCCCK

FEBRUARY 10, 2011
VOLUME 115
NUMBER 5
pubs.acs.org/JPCC

THE JOURNAL OF PHYSICAL CHEMISTRY C

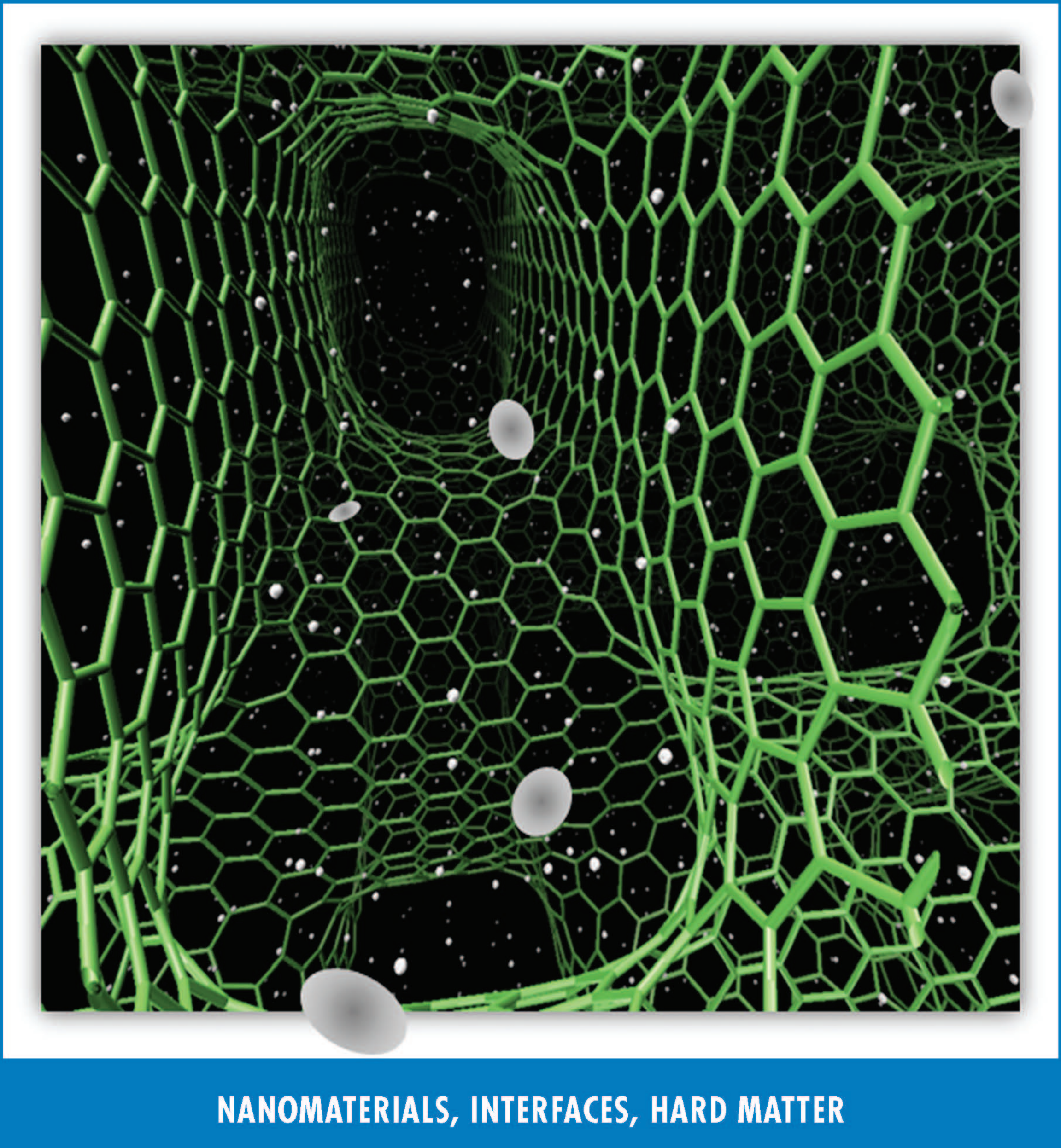

Depiction of Carbon Nanofoam with Properly Sized Pores and Channels for Hydrogen Storage (see page XA)

NANOMATERIALS, INTERFACES, HARD MATTER

ACS Publications
MOST TRUSTED. MOST CITED. MOST READ.

www.acs.org

THE JOURNAL OF PHYSICAL CHEMISTRY C

ARTICLE

pubs/acs/org/JPCC

Hydrogen Storage Capacity of Carbon-Foams: Grand Canonical Monte Carlo Simulations

Abhishek K. Singh,[†,‡,#] Jianxin Lu,[†,#] Rachel S. Aga,[§] and Boris I. Yakobson[*,†]

[†]Department of Mechanical Engineering and Materials Science, Department of Chemistry, and The Richard E. Smalley Institute for Nanoscale Science and Technology, Rice University, Houston, Texas 77005, United States

[‡]Materials Research Centre, Indian Institute of Science, Bangalore, India, 560012

[§]Department of Chemistry, Wright State University, Dayton, Ohio 45435-0001, United States

S *Supporting Information*

ABSTRACT: Hydrogen storage in the three-dimensional carbon foams is analyzed using classical grand canonical Monte Carlo simulations. The calculated storage capacities of the foams meet the material-based DOE targets and are comparable to the capacities of a bundle of well-separated similar diameter open nanotubes. The pore sizes in the foams are optimized for the best hydrogen uptake. The capacity depends sensitively on the $C-H_2$ interaction potential, and therefore, the results are presented for its “weak” and “strong” choices, to offer the lower and upper bounds for the expected capacities. Furthermore, quantum effects on the effective $C-H_2$ as well as H_2-H_2 interaction potentials are considered. We find that the quantum effects noticeably change the adsorption properties of foams and must be accounted for even at room temperature.

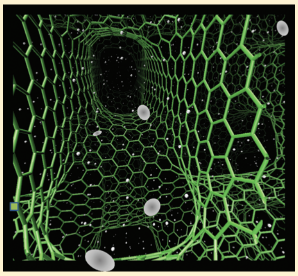

1. INTRODUCTION

Hydrogen is a source of clean and renewable energy and is considered to be an alternative to fossil fuel. One of the major hurdles to its practical usage is a lack of storage media, which could meet the DOE 2015 targets,[1] i.e., gravimetric $g > 5.5$ wt % and volumetric $v > 40$ kg/m^3 (to appreciate the challenge, this is greater than the half-density of liquid hydrogen of 71 kg/m^3, at 20 K). This has led to an extensive search for materials, which can store hydrogen within a reasonable volume without significant increase in weight. Among the various promising candidates, carbon based nanomaterials have received special attention[2−5] because they are lightweight and have a high surface-to-volume ratio. Additionally, for efficient reversible storage within the achievable temperatures and pressures by existing technology, the adsorption energy should be in the range of 0.01−0.5 eV/H. Owing to their ability to bind hydrogen both by physisorption and chemisorption, graphitic structures can satisfy the required binding energy criterion.

Although carbon nanotubes (CNT) are considered promising for hydrogen storage,[2,6,7] CNT almost always form bundles thereby reducing their hydrogen uptake. The shorter tube−tube distances (3.4 Å) in the bundles hinder the hydrogen molecule from accessing the space between tubes, while the interior is also usually blocked. It has been shown theoretically that a wall-to-wall separation close to 0.8−1.0 nm[8−10] would be best for the hydrogen storage in CNT bundles.[9,11] However, synthesizing and stabilizing bundles with such separation is challenging if at all possible. This is also true for graphene, where layers separated by more than 0.8 nm could store significant amounts of hydrogen;[12−14] yet, such spacing of the layers so far appears unfeasible for experimental realization.

In the case of 3D carbon nanoporous materials, it has been shown that a pore size ∼1 nm could be ideal for storage.[11,13,15] There are several 3D carbon foams,[9,10,16−18] both experimentally[16,18,19] produced and theoretically[9,10,14,20−22] proposed. However, the experimentally synthesized foams often have very large pore sizes, whereas theoretically discussed foams often lack any suggested way of making them. Recently, we discussed[9] a carbon foam achievable via a known welding technique[20,23,24] from crossed carbon nanotubes. These foams are almost isotropic, stable, and mechanically as stiff as steel in all directions.[9] The abundance of pores in these foams makes them ideal for hydrogen storage, whereas their architecture is well-defined and can be designed in a systematic manner. Even if not made directly, such foams can be useful as a representative model system for studying storage in practical nanoporous materials with a usually known recipe and measured surface area but very little data about their atomic makeup (activated carbons, aerogels, and nanoporous and amorphous carbons[19]).

With this in mind, we designed a series of 3D carbon foams using different CNTs, aiming to assess the volumetric and gravimetric capacities and to find the optimum storage. Grand canonical Monte Carlo (GCMC) simulations are used, with the judicious choice of interaction potentials, to estimate the storage capacities under ambient conditions. The storage capacity of such foams is compared with the well-separated CNT bundles. The mass

Received: May 27, 2010
Revised: November 8, 2010
Published: November 30, 2010

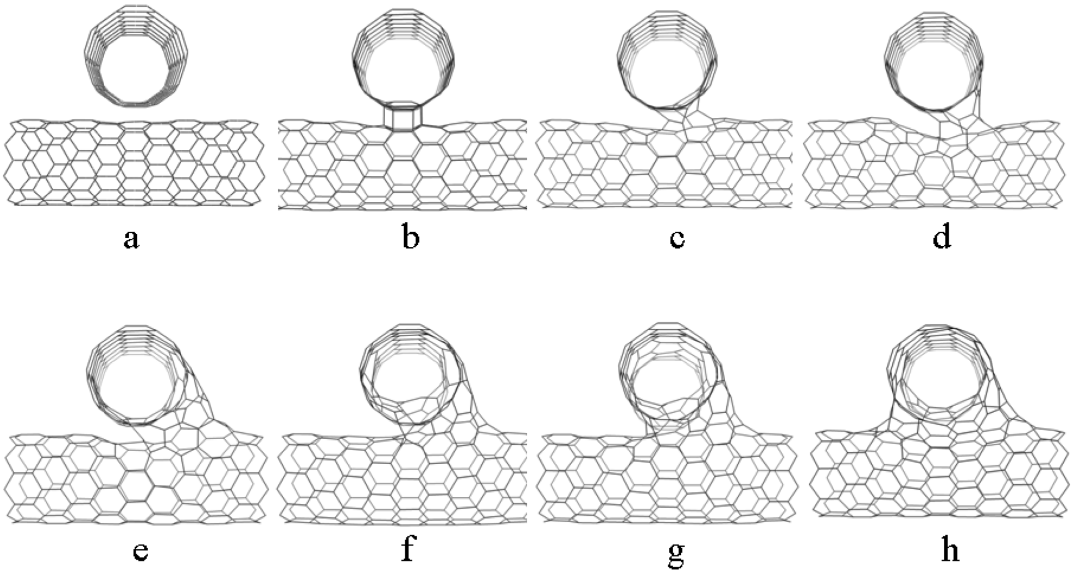

Figure 1. (a−h) Representative configurations during the welding process of (5,5) and (9,0) nanotubes. Panel a shows the starting configuration.

densities and pore sizes are optimized for the hydrogen uptake. Due to light weight of H_2 and low storage temperature, the quantum effects on the C−H_2 as well as H_2−H_2 interaction potentials are considered, and their consequences on the storage are evaluated.

2. GENERATION OF FOAM STRUCTURES

Carbon foams are designed by welding single-wall carbon nanotubes, SWNT.[9] In order to obtain a foam, an armchair and a zigzag SWNT of similar diameters are chosen as shown in Figure 1a. While the similarities in diameters ensure the uniformity of foams in *x* and *y* directions, the choice of different chiralities ensures the A−A stacking at the crossing interface contact, when in the starting configuration the tubes are placed perpendicular to each other. The facing C−C pairs in the central part of the interface are brought to 1−1.5 Å, to the C−C bond length (that is pressed to each other, to initiate the welding coalescence). If the spacing is too large, the connection cannot be built, whereas at too small distances, the tubes fuse very quickly leading to a nonuniform "fat" neck, which is also undesirable.

As a next step we construct a unit cell of foam via a welding process. In each step, the most energetically preferred bond in the tube junction is rotated by 90° via Stone−Wales (SW) transformation,[25] followed by relaxation of the whole structure. During the relaxation process, the tubes' edges are fixed to prevent them from becoming parallel to each other. The process continues until the neck becomes thick and a smoothly curved junction is formed. For the optimization process, we use conjugate gradient method with the Tersoff−Brenner interaction potential for carbon.[26] These calculations are computationally too demanding to be handled by quantum mechanical methods such as density functional theory based methods. At the same time, the structural properties obtained from using the Tersoff−Brenner potential agree very well with the DFT results. Snapshots of welding process are shown in Figure 1a−h.

The computed energies of the structures at each step of the welding process are plotted in Figure 2. The letters mark the local minima and correspond to structures in Figure 1a−h. Clearly, the junction formation is thermodynamically favorable, provided sufficient pressure, and should be kinetically achievable at an elevated temperature and especially when irradiated.

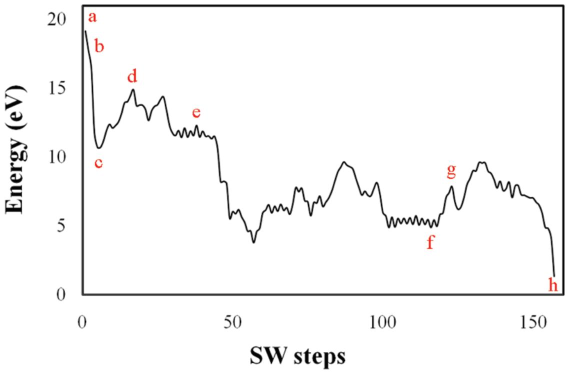

Figure 2. Total energy of the structure during the welding process of (5,5) + (9,0) tubes. Letters mark the structures shown in the Figure 1.

We note that while topology does require no less than 12 heptagons upon the neck formations, a few excessive defects (pentagons and accordingly extra heptagons) emerge in the welding process. As an example, a pentagon−heptagon pair as 5|7 dislocation is highlighted in Figure 3. In such cases, a balls-end bond 90° rotation moves the dislocation (to Figure 3b), until the pentagon-heptagon pair meets another heptagon (Figure 3b), thereby removing the excess-dislocation and leaving only a heptagon (Figure 3c). The process is continued until all of the extra defects are removed and the junction with 12 heptagons is formed,[27] following Euler's rule.

. In order to attempt a systematic comparison of the storage capacities of different foams, we generated two families of foams as shown in Figure 4: one isodensity, with constant mass density, and another one geometrically similar, where tubes, pores, and channels all scale up roughly in proportion.

3. GRAND CANONICAL MONTE CARLO SIMULATIONS

The storage capacities are calculated using GCMC simulations, with empirical interatomic potentials. GCMC is a powerful

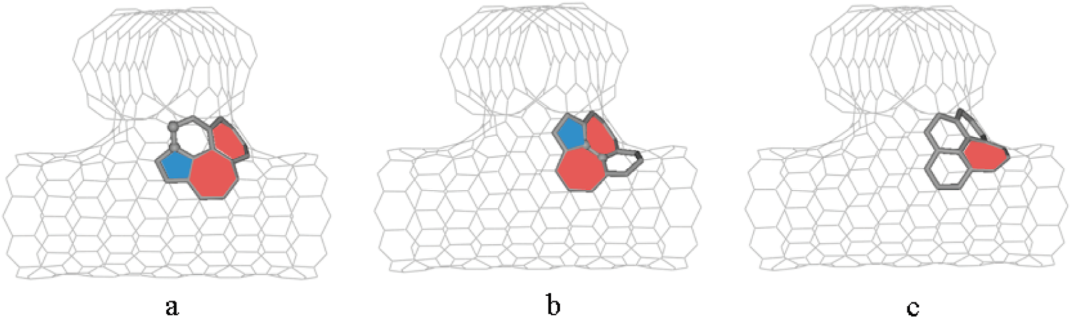

Figure 3. Example sequence of the extra 5|7 removal process from the junction of (5,5) + (9,0) tubes.

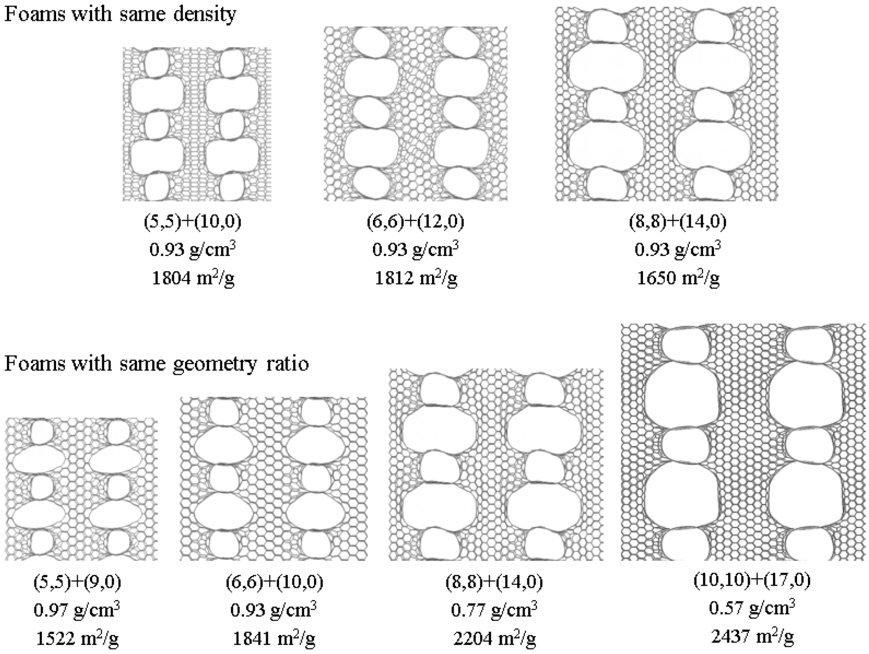

Figure 4. Structures of the foams belonging to the two families, isodensity (top) and geometrically similar (bottom). The corresponding precursor-nanotube types, density (g/cm^3), and accessible surface area (ASA, m^2/g) are marked.

technique used to estimate the ambient condition storage by explicitly accounting for density fluctuations at fixed volume and temperature. This is achieved by means of trial insertion and deletion of molecules, H_2. At first, a random trial attempt is made for choosing between the particle insertion and deletion. In the case of insertion, a particle is placed with uniform probability density, whereas for deletion one of the N particles is randomly deleted. The trial is accepted or rejected according to their grand canonical weighting.

The simulations are carried out in 3D cells, with the periodic boundary conditions employed to exclude the surface effects. The positions of the C atoms of the foam are fixed. The energies of the H_2 adsorption sites were calculated classically. A typical simulation consists of 10^6 steps to ensure that an equilibrium configuration was reached, followed by 2×10^6 steps to evaluate the number of hydrogen molecules N_{H_2} in the considered volume. The simulations are performed at three different temperatures of 77, 150, and 298 K and in a pressures range of 0.01−10.24 MPa (divided into 11 points). The center of mass of the molecule is used to describe the position of H_2.

For the hydrogen storage, the total capacities include also the hydrogen that would be there even in the absence of the sorption materials. In order to get a more instructive metric of material-related adsorption storage, one defines excess capacity as the stored hydrogen in the system minus the storage in the same volume in the absence of any sorption media. The resulting number of hydrogen molecules used to calculate the wt. % and vol. %.

3.1. Interaction Potentials. The storage capacity depends on the choice of $C-H_2$ interaction potential and is sensitive to the $C-H_2$ binding energy. Such empirical potentials are obtained by fitting either experimental adsorption data or ab initio adsorption energy. There is a clear lack of consensus regarding the potential, which reproduces the experimental results flawlessly. Our aim here is to estimate the storage potential of the 3D foams as reasonably close to experiments as possible. In this work, we have selected two different $C-H_2$ potentials,[12,28] which are used extensively in the literature. This allows us to analyze how much the variability in the potential affects the storage. Results obtained by choosing only one type of model would have been not very reflective of the actual storage in the foam. One of the interaction potentials was proposed by Wang et al.[28] It has a 12−6 Lennard-Jones form, with parameters chosen to fit the energy spectra from scattering experiments of H_2 physisorbed on graphite

$$u(r) = 4\varepsilon[(\sigma/r)^{12} - (\sigma/r)^{6}]$$

where $\varepsilon = 3.7$ meV/molecule and $\sigma = 3.0$ Å. The other potential has an empirical Buckingham form proposed by Patchkovskii et al.[12]

$$u(r) = Ae^{-\alpha r} + C_6 r^{-6}$$

where $A = 1100$ eV/molecule, $C_6 = -17$ eV Å^6/molecule, and $\alpha = 3.6/$ Å.

In spite their similar forms, the potential of Patchkovskii et al.[12] gives a stronger C−H_2 binding and results in higher absorption compared with the more conservative results obtained with the potential of Wang et al.[28] Accordingly, we call them strong[12] and weak,[28] and the storage capacities obtained by using these two potentials offer the upper and the lower bond for expected realistic experimental range. This range arises solely because of the differences of the C−H_2 interaction potentials; and it is not related to the intrinsic actual storage capacity, which will be a constant number. For H_2−H_2 interactions, we use the Silvera−Goldman potential,[29] which treats the hydrogen molecule as single particle with no rotational degrees of freedom. In a recent study[13] it has been shown by first-principles calculations that the configurations with different H_2 orientations have comparable absorption energy, which, together with rapid thermal rotational motion, justifies approximating the H_2 molecule as a single particle.

3.2. Quantum Corrections. For a light molecule like hydrogen at low temperature, the quantum effects can be significant. By considering the quantum effects in hydrogen isotopes it has been shown that heavier isotopes are adsorbed stronger than lighter ones.[30] By comparing the thermal de Broglie wavelength of a particle of mass m, $\Lambda = (\beta h^2/2\pi m)^{1/2}$ where $\beta = 1/k_B T$, k_B being the Boltzmann constant, and T the temperature with the mean pore size a, the validity of the classical treatment can be tested. The classical treatment is justified only for the cases where $\Lambda/a \ll 1$.

The quantum effects can be incorporated by elegant Feynman and Hibbs variational treatment,[31] where a quantum particle of mass m is characterized by a Gaussian spread with a thermal quantum width Λ, around the particle center of mass. The corresponding partition function of an assembly of N such particles can be expressed as

$$Z_{\mathrm{FH}} = \frac{1}{N!}\left(\frac{2\pi m}{\beta}h^2\right)^{2N/2}\int\dots\int \mathrm{d}\bar{r}_1\dots\mathrm{d}\bar{r}_N \exp\left[-\beta\sum_{i<j}U_{\mathrm{FH}}(r_{ij})\right] \qquad (1)$$

where

$$U_{\mathrm{FH}}(r) = \left(\frac{24\pi\mu}{\beta}h^2\right)^{3/2}\int \mathrm{d}\bar{R}\, U(|\bar{r}+\bar{R}|) \exp\left(\frac{24\pi^2\mu}{\beta}h^2R^2\right) \qquad (2)$$

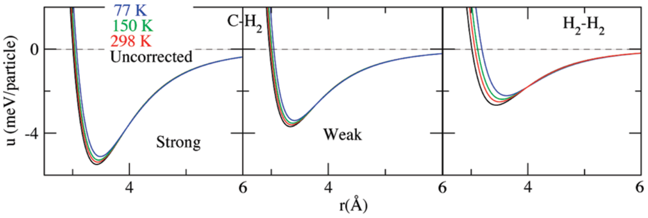

Figure 5. C−H_2 and H_2−H_2 interaction potentials, purely classical (black), and incorporating the quantum effects at T = 77 (red), 150 (green), and 298 K (blue). The strong[12] and weak[28] potential choices for C−H_2 are shown separately. The quantum effects weaken the binding by the amount inversely proportional to T.

is the average effective potential between a pair of particles (reduced mass $\mu = m/2$), incorporating the spread in the position due to the uncertainty principle. An expansion of eq 2 leads to the accurate expression of the quadratic Feynman−Hibbs (QFH) potential[31]

$$U_{\mathrm{FH}}(r) = U(r) + \frac{\beta h^2}{96\pi^2\mu}\left[U''(r) + \frac{2U'(r)}{r}\right]$$

where the prime and double prime are the first and second r derivatives, respectively. C−H_2 and H_2−H_2 corrections depend on temperature, with the QC in C−H_2 being less significant. Effectively, quantum corrections add some repulsion as shown in Figure 5.

3.3. Accessible Surface Area. Surface area is an important and commonly used parameter, related to the adsorption capacity of the media. Generally, surface areas are measured by the Brunauer, Emmet, and Teller (BET) method via N_2 adsorption isotherms. The BET method via N_2 may introduce errors because it assumes multilayer adsorption that is not the case for H_2. Furthermore, there are pores with small size where N_2 cannot enter when H_2 still can due to the differences in their effective size. Therefore BET surface area calculated via N_2 adsorption cannot be very precise for the evaluation of hydrogen storage. We calculate the accessible surface area (ASA), which is geometrically obtained by "rolling" a probe molecule along the surface of the porous media.[32] By choosing the diameter of the probe molecule to be the same as that of the adsorbent, a more relevant estimate of the surface area can be obtained. We choose H_2 as the probe molecule to estimate the ASA, which is given in the Figure 4. The error obtained by the "rolling" method is practically negligible.

4. RESULTS AND DISCUSSION

First, we compare the storage capacity of the selected foam with the well-spaced same-diameter nanotube bundles. For this, we choose one foam previously generated by Ding et al.[9] from the crossed (5,5) + (10,0) nanotubes (we use symbol "+" resembling the cross-orientation of the precursor tubes). The bundles are generated by packing the (10,0) nanotubes in a triangular lattice and varying the wall-to-wall distance (D) within a bundle series. The excess volumetric and gravimetric capacities of these bundles are shown in Figure S1. The gravimetric fraction increases monotonically with the increasing tube−tube separation; however, the volumetric capacity peaks at D = 9 Å. The metrics for the foam are also shown in Figure S1. The maximum of volumetric ratio in the foam is obtained at T = 77 K and 1 MPa, which compares very well with the corresponding maxima of the tube bundles as shown in Figure 6. Although they have similar storage

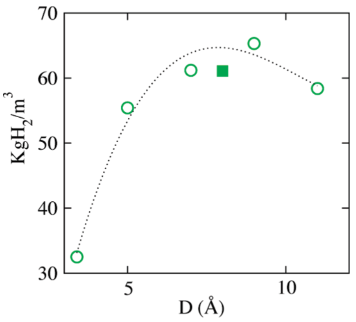

Figure 6. Green circles in the plot represent the maxima of the volumetric capacity for the tube bundles as a function of the wall-to-wall distance *D* at *P* = 1.28 MPa and *T* = 77 K. The solid square represents the corresponding maximum for the (5,5) + (10,0) foam. The values are obtained using strong potential.

capacity, to synthesize a bundle of well-aligned tubes with uniform spacing of 9 Å is unfeasible. Normal tube−tube distances in the bundles are ∼3.4 Å, and the storage capacity is far below that of the foams, Figure S1. The superiority of foams over the tube bundles is due to their better architecture, which ensures the accessibility and uniformity of the pores. A partial advantage is also from the availability of better attraction sites for hydrogen around the neck area of the foams, due to enhanced curvature. Figure S1 also demonstrates the effect of the two interaction potentials used in this study. Clearly, due to a weaker C−H_2 binding strength in the Wang potential, the wt. % and density of adsorbed hydrogen is systematically lower than the corresponding adsorption result from the "strong" Patchkovskii potential. Because of the lack of experimental data for adsorption of H_2 molecules on foams, the accuracy of these potentials cannot be easily validated. However, the results obtained from these two potentials can serve as a range in which the experimental value will lie. Therefore, we report the storage data obtained for both potentials.

Besides being a good media for hydrogen storage, 3D carbon foam offers an opportunity to generate structures with the desired pore sizes. This can be achieved by the adequate choice of the tube diameter and the separation between the necks. A series of foams can be obtained by varying these parameters. Here we choose two different foam families as discussed above and shown in Figure 4.

The storage capacities of the foams with the same mass density are evaluated and shown in Figure 7. In this isodensity family, the diameters are varied while keeping the mass density of the foam material constant. We generated three such foams, namely, (5,5) + (10,0), (6,6) + (12,0), and (8,8) + (14,0). The choice of chiralities minimizes the difference in the diameter of the crossing tubes, to ensure the uniformity of the pores. The gravimetric and volumetric storage capacities peak for the different types of foams, respectively. The maximum gravimetric capacities obtained for these foams at different temperatures and pressures are shown in Figure 7. Gravimetric capacity peaks for the (6,6) + (12,0) foam as shown in Figure 7, bottom right. This must be due to the optimal distances between the walls of the precursor tubes as well as between the formed necks. These parameters are close to 1 nm, which is optimal for storage capacities.

Next we studied the adsorption of H_2 molecule in the other family of foams, where the pore sizes were varied in the geometric proportion. Four such foams were generated by the method described in the previous section. The structures are shown in the lower panel of Figure 4, and the corresponding storage capacities are shown in Figure S2. The storage capacities show systematic behavior. The trends for maximum gravimetric and volumetric capacity are shown in Figure 8. The gravimetric % increases monotonically; however, the volumetric measure peaks again with the (6,6) + (10,0) foam. The volumetric as well as gravimetric capacities follow a similar trend as ASA/volume and ASA/g, respectively, the upper panel of Figure 8. This is an important connection as the foams can be optimized by measuring the

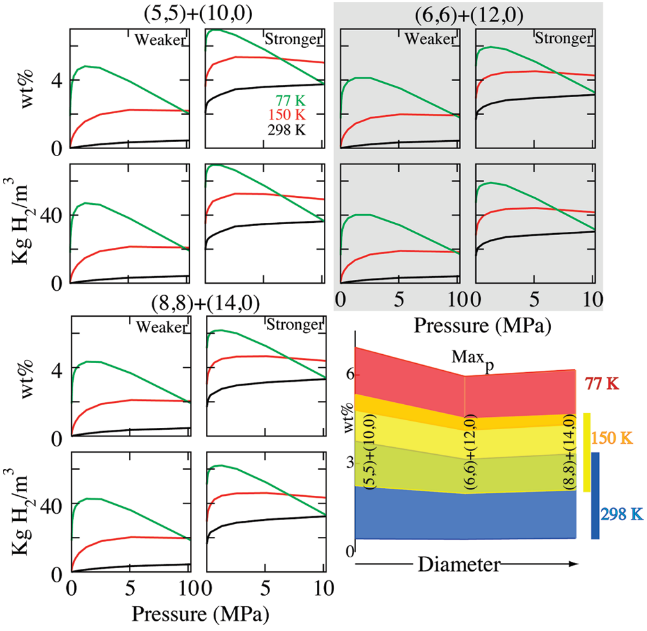

Figure 7. Gravimetric % and volumetric measure of H_2 in the nanofoams with the constant densities, obtained by GCMC. The left and right plots are obtained using weak[28] and strong[12] C−H_2 potentials. The lower right panel shows the maxima of gravimetric % of H_2 in the foams at different temperatures and pressures obtained by GCMC. The red, yellow, and blue colors show the wt. % calculated at 77, 150, and 298 K, respectively. The band within a color show the range of storage obtained with the use of weak and strong interaction potentials.

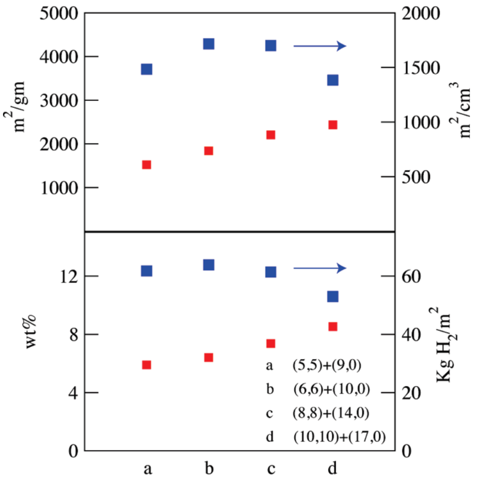

Figure 8. Upper panel, accessible surface area per volume and per gram of foam material with the proportionate pore size (family of geometrically similar). Lower panel, corresponding maxima of volumetric and gravimetric capacity of foams.

Table 1. Storage Capacity Overestimates (in %) of Purely Classical Simulations Relative to the Corrected for Quantum Effects, for (10,10) + (17,0) Foam

	classical overestimates by (%) (2.56 MPa)	
T (K)	wt total	wt excess
298	2.45 (weak)−3.18 (strong)	4.55−7.01
150	9.35−9.84	10.63−12.89
77	17.47−19.35	19.44−22.34

surface areas per volume before doing actual adsorption experiments.

Finally, for the lighter molecules where the de Broglie wavelength could be significant, inclusion of the quantum effects is necessary. We incorporate the quantum effects in the interaction potentials. With the inclusion of the quantum corrections, the effective interaction potentials become temperature dependent, as seen in Figure 5. The quantum corrected $C-H_2$ (both strong and weak) as well as H_2-H_2 Silvera−Goldman potentials are shown in Figure 5. The effective radius of the H_2 molecule increases at lower temperatures essentially reducing the depth of the attractive part of the potential. This reduces the storage capacity of the foams (or any other adsorbing carrier).

The storage capacities of foams with the quantum corrected potentials are shown in Table 1. The quantum corrections reduce the storage capacity particularly at low temperatures. Table 1 shows the overestimation of the storage due to neglect of the quantum effects. As expected, the decrease is most significant with the decreasing temperature and increasing pressure. The hydrogen uptake can be reduced by as much as 22% at 77 K. The classical results are more accurate at increasing temperature, but the consequences of the quantum effects still should not be neglected. Even at room temperature, the storage is classically overestimated by as much as 7%. Furthermore, we also analyze the sole effect of neglecting the quantum correction in H_2-H_2 potential. We find that the major corrections are due to quantum effects in H_2-H_2 interaction potentials. Therefore, inclusions of quantum corrections are important to make realistic comparisons with the experimental storage capacities.

5. CONCLUSIONS

We designed a series of the 3D foams using a welding algorithm process, which has its analogues in experiments. We compute the storage capacities of such foams using classical GCMC simulations. These simulations are performed with the two selected types of $C-H_2$ interaction potentials (weak and strong), which sets the range for the storage capacity prediction. Storage parameters depend sensitively on the choice of the interaction potential. For comparison, we also simulate the storage capacities of the idealized open nanotube bundles with varying tube−tube distance. We find the storage capacities of the foams to be comparable to similar diameter nanotube bundles. Two families of foams are generated, one with constant mass density (isodensity) and another of nearly unvarying shape (geometrically similar). The foams are optimized for best storage capacity within both of the families. Furthermore, we study the consequences of quantum effects on storage capacities. The quantum effects are incorporated in the interaction potentials via Feynman−Hibbs formulation. The quantum effects noticeably reduce the storage capacity and must be incorporated in order to make realistic predictions for the experimental systems. The foams can serve as a model for various nanoporous materials whose atomic structures are often poorly defined while their recipes and surface areas are known. Model foams with the desired surface area can be readily generated, and then their storage capacity can be quantitatively evaluated at arbitrary pressure and temperature. Furthermore, as soon as the structure is selected, the study can be extended to the diffusion and transport, including thermal, to also evaluate nonequilibrium, kinetic performance of the material. Foams thus can provide an indirect method for theoretically assessing the feasibility and performance of carbon nanoporous materials.

ASSOCIATED CONTENT

Supporting Information. Figure S1: excess gravimetric and volumetric % calculated. Figure S2: storage capacity of the family of foams with the proportionate pore size. This material is available free of charge via the Internet at http://pubs.acs.org.

Author Contributions

[#] These authors contributed equally to this work.

ACKNOWLEDGMENT

This work was supported by the DOE Hydrogen Sorption Center of Excellence, Contract No. DE-FC36-05GO15080, and partially by the Robert A. Welch Foundation (C-1590). One of us (J.L.) is grateful to Feng Ding for guidance with the structures simulations.

REFERENCES

(1) Targets for Onboard Hydrogen Storage Systems for Light-Duty Vehicles, 2009; http://www1.eere.energy.gov/hydrogenandfuelcells/storage/pdfs/targets_onboard_hydro_storage_explanation.pdf.

(2) Dillon, A.; Jones, K.; Bekkedahl, T.; Kiang, C.; Bethune, D.; Heben, M. *Nature* **1997**, *386*, 377.

(3) Atkinson, K.; Michael, R. *Fuel Cells Bull.* **2001**, *4*, 9.

(4) Singh, A. K.; Ribas, M. A.; Yakobson, B. I. *ACS Nano* **2009**, *3*, 1657.

(5) Kowalczyk, P.; Holyst, R.; Terrones, M.; Terrones, H. *Phys. Chem. Chem. Phys.* **2007**, *9*, 1786.

(6) Yin, Y.; Mays, T.; McEnaney, B. *Langmuir* **2000**, *16*, 10521.

(7) Williams, K.; Eklund, P. *Chem. Phys. Lett.* **2000**, *320*, 352.

(8) Leonard, A. D.; Hudson, J. L.; Fan, H.; Booker, R.; Simpson, L. J.; O'Neill, K. J.; Parilla, P. A.; Heben, M. J.; Pasquali, M.; Kittrell, C.; Tour, J. M. *J. Am. Chem. Soc.* **2008**, *131*, 723.

(9) Ding, F.; Lin, Y.; Krasnov, P.; Yakobson, B. *J. Chem. Phys.* **2007**, *127*, 164703.

(10) Weck, P. F.; Kim, E.; Balakrishnan, N.; Cheng, H.; Yakobson, B. I. *Chem. Phys. Lett.* **2007**, *439*, 354.

(11) Wang, Q.; Johnson, J. *J. Chem. Phys.* **1999**, *110*, 577.

(12) Patchkovskii, S.; Tse, J.; Yurchenko, S.; Zhechkov, L.; Heine, T.; Seifert, G. *Proc. Natl. Acad. Sci. U.S.A.* **2005**, *102*, 10439.

(13) Aga, R. S.; Fu, C. L.; Krcmar, M.; Morris, J. R. *Phys. Rev. B* **2007**, *76*, 165404.

(14) Kuchta, B.; Firlej, L.; Cepel, R.; Pfeifer, P.; Wexler, C. *Colloids Surf., A* **2010**, *357*, 61.

(15) Gu, C.; Gao, G.-H.; Yu, Y.-X.; Mao, Z.-Q. *Int. J. Hydrogen Ener.* **2001**, *26*, 691.

(16) Cao, A.; Dickrell, P.; Sawyer, W.; Ghasemi-Nejhad, M.; Ajayan, P. *Science* **2005**, *310*, 1307.

(17) Umemoto, K.; Saito, S.; Berber, S.; Tomanek, D. *Phys. Rev. B* **2001**, *64*, 193409.

(18) Yang, Z.; Xia, Y.; Mokaya, R. *J. Am. Chem. Soc.* **2007**, *129*, 1673.

(19) Pfeifer, P.; Burress, J. W.; Wood, M. B.; Lapilli, C. M.; Barker, S. A.; S. Pobst, J.; Cepel, R. J.; Wexler, C.; Shah, P. S.; Gordon, M. J.;

Suppes, G. J.; Buckley, S. P.; Radke, D. J.; Ilavsky, J.; Dillon, A. C.; Parilla, P. A.; Benham, M.; Roth, M. W. High-Surface-Area Biocarbons for Reversible On-Board Storage of Natural Gas and Hydrogen; *Mater. Res. Soc. Symp. Proc.* Warrendale, PA, 2008.

(20) Zhao, Y.; Smalley, R.; Yakobson, B. *Phys. Rev. B* **2002**, *66*, 195409.

(21) Deng, W.-Q.; Xu, X.; Goddard, W. *Phys. Rev. Lett.* **2004**, *92*, 166103.

(22) Dimitrakakis, G. K.; Tylianakis, E.; Froudakis, G. E. *Nano Lett.* **2008**, *8*, 3166.

(23) Zhao, Y.; Lin, Y.; Yakobson, B. I. *Phys. Rev. B* **2003**, *68*, 233403.

(24) Zhao, Y.; Yakobson, B. I.; Smalley, R. E. *Phys. Rev. Lett.* **2002**, *88*, 185501.

(25) Stone, A.; Wales, D. *Chem. Phys. Lett.* **1986**, *128*, 501.

(26) Brenner, D. *Phys. Rev. B* **1990**, *42*, 9458.

(27) Crespi, V. *Phys. Rev. B* **1998**, *58*, 12671.

(28) Wang, S.; Senbetu, L.; Woo, C. *J. Low Temp. Phys.* **1980** *41*, 611.

(29) Silvera, I.; Goldman, V. *J. Chem. Phys.* **1978**, *69*, 4209.

(30) Beenakker, J. J. M.; Borman, V. D.; Krylov, S. Y. *Chem. Phys. Lett.* **1995**, *232*, 379.

(31) Feynman, R. P.; Hibbs, A. R. *Quantum Mechanics and Path Integrals*; McGraw-Hill: New York, 1965.

(32) Frost, H.; Düren, T.; Snurr, R. Q. *J. Phys. Chem. B* **2006**, *110*, 9565.